Nonlinear dynamics of the wolf tone production

Etienne Gourc, Christophe Vergez, Pierre-Olivier Mattei, Samy Missoum

Nonlinear dynamics of the wolf tone production

Etienne Gourc[a,*], Christophe Vergez[a], Pierre-Olivier Mattei[a], Samy Missoum[b]

[a] *Aix Marseille University, CNRS, Centrale Marseille, LMA, Marseille, FRANCE*
[b] *Department of Aerospace and Mechanical Engineering, University of Arizona, Tucson, Arizona, USA*

Abstract

Some bowed string instruments such as cello or viola are prone to a parasite phenomenon called the wolf tone that gives rise to an undesired warbling sound. It is now accepted that this phenomenon is mainly due to an interaction between a resonance of the body and the motion of the string. A simple model of bowed string instrument consisting of a linear string with a mass-spring boundary condition (modeling the body of the instrument) and excited by Coulomb friction is presented. The eigenproblem analysis shows the presence of a frequency veering phenomenon close to 1 : 1 resonance between the string and the body, giving rise to modal hybridation. Due to the piecewise nature of Coulomb friction, the periodic solutions are computed and continued using a mapping procedure. The analysis of classical as well as non-smooth bifurcations allows us to relate warbling oscillations to the loss of stability of periodic solutions. Finally, a link is made between the bifurcations of periodic solutions and the minimum bow force generally used to explain the appearance of the wolf tone.

1. Introduction

Players of bowed string instruments might experience difficulties to produce a steady tone of good quality for certain ranges of playing parameters, regardless of the quality of the instrument. This phenomenon, mainly occurring with cellos is generally referred to as the wolf tone in the musical community and is characterized by a distinct warbling sound. There have been many attempts to explain the phenomenon. Among the first, White [1] showed that the wolf tone occurs when the played note coincides with a strong resonance of the body of the instrument. Almost at the same time, Raman [2] recorded the motion of the string during the wolf tone using optical lever, and suggested that the sympathetic resonance of the body of the cello takes energy from the string, causing cyclic alternance of bowed string motion and was the first to introduce the notion of minimum bow force. This notion was later revisited by Schelleng [3] who formulated maximum and minimum bow force limits as a function of the playing parameters for which Helmholtz motion can take place. In order to account for the dynamic of the body, Schelleng introduced a resistance parameter and showed that the minimum bow force is affected by this resistance. It is however quite difficult to give a physical interpretation of this resistance parameter and Woodhouse revisited the formula to incorporate the measured body behavior [4].

Since then, considerable efforts have been made to derive accurate models of bowed string instruments. Some of the necessary ingredients, such as the string bending stiffness, finite width

*Corresponding author

Email addresses: etienne.gourc@gmail.com (Etienne Gourc), vergez@lma.cnrs-mrs.fr (Christophe Vergez), mattei@lma.cnrs-mrs.fr (Pierre-Olivier Mattei), smissoum@arizona.edu (Samy Missoum)

of the bow or the frictional behavior of the rosin are presented in [5]. Inacio [6] developed a modal model of bowed string instrument able to incorporate measured or simulated body behavior. They were able to reproduce the behavior of the cello at the wolf region, and showed the dependence of the beating frequency on the bowing parameters. A linear stability analysis of this model is presented in [7]. A similar model was used to investigate the effect of wolf killing device in [8]. Mansour used a digital wave-guide modelling approach to analyze the behavior of plucked and bowed string instruments [9]. They also revised the minimum bow force [10] formula accounting for the fact that close to the wolf region, the force transmitted at the bridge departs from the assumed perfect sawtooth considered in earlier minimum bow force calculation. They revealed that when the played note is close to the body resonance frequency, the dependence of the minimum bow force on the playing parameters is complex and deviates from the original Schelleng's diagram.

The previous mentioned studies involve either strong hypothesis on the behavior of the system allowing to make analytical predictions or complex model needing intensive numerical calculation. Although bowed string instruments exhibit strong nonlinear behavior due to the essential nonlinear nature of friction, very few studies analyzed the bifurcation behavior of these systems. Friedlander studied a model of non-dissipative string with rigid terminations, bowed at single point at an integer fraction of the string length and showed that for this simple model, all periodic solutions are unstable [11]. It has been shown later that this instability was due to the absence of dissipation on the model [12]. In musical acoustics, methods dedicated to the analysis of nonlinear dynamical systems such as continuation methods have been mostly used to investigate the behavior of wind instruments. The software DDE-biftool [13] has been used to investigate the periodic solution and bifurcations of flute-like instruments in [14]. The oscillation threshold of a clarinet as a function of model parameters has been investigated in [15]. Properties of saxophone bifurcation diagrams have been investigated in [16, 17]. A bifurcation diagram based classification of different models of trumpets has been proposed in [18]. To the authors' knowledge, the only study investigating the bifurcation behavior of bowed string instruments is presented in [19]. They used the continuation software Manlab [20] and a regularized friction model to compute the bifurcation diagram of a toy model of bowed string instrument consisting of two string modes. They showed the existence of period doubling bifurcation yielding to a first register Helmholtz motion. Although these methods are mostly suited to analyze low dimensional, simplified models, they allow one to extract essential features of the dynamics of the system. A key feature which certainly explains the lack of nonlinear analysis of bowed string instruments is the discontinuous nature of friction which is generally not compatible with available software.

The present paper is devoted to the analysis of string body interaction in the wolf tone region, using a simplified model of bowed string instrument. In the second section, the toy model of cello is presented. The conservative partial differential equation is projected, by using a standard Galerkin method, on a real modal basis, prior to adding modal damping. In the third section, numerical simulations are used to demonstrate that this simple model is able to reproduce warbling oscillations, characteristic of the wolf tone. In the fourth section, we present the mapping procedure to compute the periodic solutions and their stability. The special case of grazing bifurcation, encountered for non-smooth dynamical systems is also addressed. In section five, the bifurcation diagrams obtained for bowing parameters in the vicinity of $1:1$ resonance between the string and the body are presented. It is shown that bifurcations of the periodic stick-slip motion are responsible for beating oscillations. Finally, we show that the bifurcations of periodic solutions may also be interpreted in term of minimum bow force.

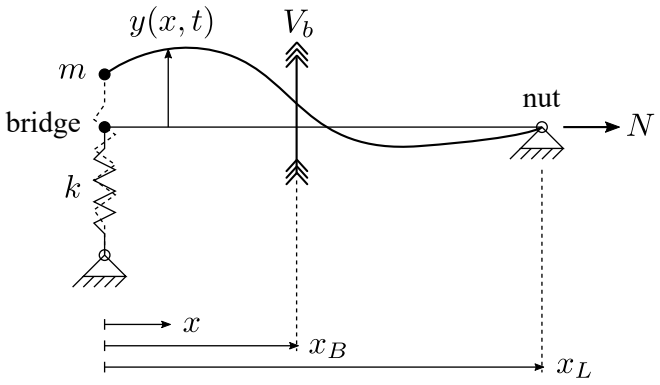

Figure 1: Simplified model of cello

2. Description of the model

The simplified cello model is depicted in Fig. 1. It consists of a linear string connected at the origin to a linear oscillator of mass m and stiffness k, representing the dynamic of the body. The string has a variable effective length $x_L \in [0, L]$, where L is the distance from the bridge to nut. It is subjected to a pre-stress tensile force N and its mass per unit length is denoted by ρ. The bow with constant velocity V_b exerts a friction force at a distance x_B from the origin.

2.1. Equation of motion and boundary conditions

Denoting by $y(x,t)$ the transverse displacement of the string, the linearized equations of motion are given by

$$Ny''(x,t) - \rho\ddot{y}(x,t) + F_N\mu(\dot{y}(x,t))\delta(x - x_B) = 0 \tag{1}$$

The dots and the primes denote differentiation with respect to time and position, respectively. $\delta(x)$ is the Dirac delta, F_N the normal bow force and $\mu(\dot{y})$ the Coulomb's friction coefficient defined by

$$\mu(\dot{y}) \begin{cases} = \mu_d & \text{if } \dot{y}(x_B,t) < V_b \\ \in]-\mu_s, \mu_s[& \text{if } \dot{y}(x_B,t) = V_b \\ = -\mu_d & \text{if } \dot{y}(x_B,t) > V_b \end{cases} \tag{2}$$

where μ_d and μ_s refer to the dynamic and static friction coefficient, respectively. The geometric boundary condition at $x = x_L$ (nut) is defined by $y(x_L,t) = 0$. The mechanical boundary condition at $x = 0$ (bridge), describing the connection between the string and the body, is given by

$$Ny'(0,t) = -ky(0,t) - m\ddot{y}(0,t) \tag{3}$$

Non-dimensional quantities are introduced as

$$\begin{gathered} \tilde{x} = \frac{x}{L}, \quad \tilde{x}_L = \frac{x_L}{L}, \quad \tilde{x}_B = \frac{x_B}{L}, \quad \tilde{y} = \frac{y}{L}, \quad \tilde{t} = \tilde{\omega} = \frac{1}{L}\sqrt{\frac{N}{\rho}}t \\ \tilde{m} = \frac{m}{\rho L}, \quad \tilde{k} = \frac{kL}{N}, \quad F = \frac{F_N}{N}, \quad V = V_b\sqrt{\frac{\rho}{N}} \end{gathered} \tag{4}$$

Using Eq. (4), the non-dimensional equation of motion is given by (the tilde have been omitted for brevity)

$$y''(x,t) - \ddot{y}(x,t) + F\mu(\dot{y}(x,t))\delta(x - x_B) = 0 \tag{5}$$

Now the dots and the primes denote differentiation with respect to the non-dimensional time and position, respectively. The non-dimensional mechanical boundary condition is given by

$$y'(0,t) = -ky(0,t) - m\ddot{y}(0,t) \tag{6}$$

2.2. Modal discretization

The partial differential equation of motion Eq. (5) is discretized using modal decomposition. Neglecting the contribution of the friction force, the transverse displacement of the string is obtained through the separation of variables

$$y(x,t) = \sum_{n=1}^{N_m} Y_n(x)v_n(t) \tag{7}$$

where N_m is the number of modes retained in the modal decomposition, $v_n(t)$ the modal displacement of the n^{th} mode and $Y_n(x)$ the associated mode shape. The mode shapes are normalized using the following orthogonality condition

$$mY_n(0)Y_s(0) + \int_0^{x_L} Y_n(x)Y_s(x)dx = \delta_{ns} \tag{8}$$

where δ_{ns} is the Kroenecker delta. The unknowns of the linear eigenproblem are found by imposing $y(x,t) = Y_n(x)\mathrm{e}^{j\omega_n t}$ where $j = \sqrt{-1}$. The mode shapes are given by

$$Y_n(x) = C_n \sin(\omega_n x + \phi_n), \quad \phi_n = n\pi - \omega_n x_L \tag{9}$$

The natural frequencies ω_n are obtained as the solution of the following transcendental equation

$$(k - m\omega_n^2)\sin(\omega_n x_L) + \omega_n \cos(\omega_n x_L) = 0 \tag{10}$$

For the sake of comparison, neglecting the effect of the bridge (i.e. considering a hinge-hinged boundary conditions), the natural frequencies and mode shapes satisfies

$$\omega_n = \frac{n\pi}{x_L}, \quad \phi_n = 0, \quad C_n = \sqrt{\frac{2}{x_L}} \tag{11}$$

Substituting Eq. (7) into Eq. (5), performing Galerkin decomposition and introducing modal damping, we obtain the following modal model of the cello

$$\ddot{\boldsymbol{v}} + 2\boldsymbol{\zeta}\boldsymbol{\omega}\dot{\boldsymbol{v}} + \boldsymbol{\omega}^2\boldsymbol{v} = F\mu(\dot{y}(x_b,t))\boldsymbol{Y}(x_b) \tag{12}$$

where $\boldsymbol{v}(t) = [v_1(t), \ldots, v_{N_m}(t)]^T$, $\boldsymbol{Y}(x) = [Y_1(x), \ldots, Y_{N_m}(x)]^T$ and $\boldsymbol{\omega} = \mathrm{diag}([\omega_1, \ldots, \omega_{N_m}])$, $\boldsymbol{\zeta} = \mathrm{diag}([\zeta_1, \ldots, \zeta_{N_m}])$ gather the natural frequencies and modal damping, respectively.

2.3. Slip and stick dynamics

Before describing the dynamics of the system during sliding and sticking phases of the motion, it is convenient to rewrite Eq. (12) in state space form. Introducing the state vector $\boldsymbol{y} = [\boldsymbol{v}, \dot{\boldsymbol{v}}]^T$, Eq. (12) is expressed by

$$\dot{\boldsymbol{y}} = \boldsymbol{A}\boldsymbol{y} + \boldsymbol{b}\mu(\boldsymbol{y}) \tag{13}$$

where

$$\boldsymbol{A} = \begin{bmatrix} \boldsymbol{0}^{N_m \times N_m} & \boldsymbol{I}^{N_m \times N_m} \\ -\boldsymbol{\omega}^2 & -2\boldsymbol{\zeta}\boldsymbol{\omega} \end{bmatrix}, \quad \boldsymbol{b} = \begin{pmatrix} \boldsymbol{0}^{N_m \times 1} \\ F\boldsymbol{Y}(x_B) \end{pmatrix} \tag{14}$$

The friction coefficient is now expressed by

$$\mu(\boldsymbol{y}) \begin{cases} = \mu_d & \text{if } \boldsymbol{h}^T\boldsymbol{y} < V \\ \in]-\mu_s, \mu_s[& \text{if } \boldsymbol{h}^T\boldsymbol{y} = V \\ = -\mu_d & \text{if } \boldsymbol{h}^T\boldsymbol{y} > V \end{cases}, \quad \boldsymbol{h} = \begin{pmatrix} \boldsymbol{0}^{N_m \times 1} \\ \boldsymbol{Y}(x_B) \end{pmatrix} \tag{15}$$

2.3.1. Stick motion

During stick motion, the following condition holds

$$\boldsymbol{h}^T\boldsymbol{y} = V \tag{16}$$

such that the string and the bow velocity are equal at the bowing location. As indicated by Eq. (15), the friction coefficient does not take a steady value during sticking phases of the motion. Instead, the friction coefficient $\mu(\mathbf{y})$ varies to counteract the non-friction forces acting on the string. Multiplying Eq. (13) by $\boldsymbol{h}^T$ and substituting $\boldsymbol{h}^T\dot{\boldsymbol{y}} = 0$ from Eq. (16), we have

$$\mu(\boldsymbol{y}) = \boldsymbol{L}\boldsymbol{y}, \quad \boldsymbol{L} = -\frac{1}{\boldsymbol{h}^T\boldsymbol{b}}\boldsymbol{h}^T\boldsymbol{A} \tag{17}$$

The equation governing the dynamics of the system during the sticking phase of motion is obtained by substituting Eq. (17) into Eq. (13) as

$$\dot{\boldsymbol{y}} = \boldsymbol{R}\boldsymbol{y}, \quad \boldsymbol{R} = \boldsymbol{A} + \boldsymbol{b}\boldsymbol{L} \tag{18}$$

Equation (18) is linear and its solution can be expressed using matrix exponential as follows

$$\boldsymbol{y}(t_1) = \boldsymbol{S}(t_1 - t_0)\boldsymbol{y}(t_0), \quad \boldsymbol{S}(t_1 - t_0) = \mathrm{e}^{(t_1 - t_0)\boldsymbol{R}} \tag{19}$$

Stick-slip transition occurs at $t = t_i$ if the friction coefficient expressed by Eq. (17) exceeds the static friction coefficient μ_s giving

$$\boldsymbol{L}\boldsymbol{y}(t_i) = \pm\mu_s \tag{20}$$

2.3.2. Slip motion

We denote by slip motion, motion occurring for $\boldsymbol{h}^T\boldsymbol{y} \neq V$. Eq. (13) becomes

$$\dot{\boldsymbol{y}} = \boldsymbol{A}\boldsymbol{y} \pm \boldsymbol{b}\mu_d \tag{21}$$

Equation (21) is linear and its solution can be expressed using matrix exponential as follows

Bridge-nut string length	$L = 0.7m$
Open string natural frequency	$\omega_{string} = 2\pi \times 64.5Hz$
String mass per unit length	$\rho = 14 \times 10^{-3} kgm^{-1}$
Main body resonance frequency	$\omega_{body} = 2\pi \times 196Hz$
Main body resonance damping ratio	$\zeta_{body} = 0.7\%$
Main body resonance mobility	$M_{body} = 0.163ms^{-1}N^{-1}$
Bridge-bow distance	$0.04m$
Static friction coefficient	0.4
Dynamic friction coefficient	0.2

Table 1: Physical parameters extracted from Inacio, et al.[6]

$$\boldsymbol{y}(t_1) = \boldsymbol{M}(t_1 - t_0)\left(\boldsymbol{y}(t_0) \mp \boldsymbol{p}\right) \pm \boldsymbol{p}, \quad \boldsymbol{M}(t) = \mathrm{e}^{t\boldsymbol{A}}, \quad \boldsymbol{p} = \mp \boldsymbol{A}^{-1}\boldsymbol{b}\mu_d \tag{22}$$

Let us assume that at time $t = t_i$ we have $\boldsymbol{h}^T\boldsymbol{y}(t_i) = V$ such that the string velocity at the bowing point is equal to the bow velocity. Two scenarios are possible depending on the non friction forces acting on the string [21]. If the non friction forces acting on the string exceed the dynamic friction force, another slip motion with opposite dynamic friction coefficient takes place. On the contrary, if the non friction forces acting on the string do not exceed the dynamic friction force, stick motion is triggered. These conditions are expressed by

$$\begin{array}{ll} \text{Slip-slip transition if} & \boldsymbol{L}\boldsymbol{y}(t_i) > \mu_d \\ \text{Slip-stick transition if} & \boldsymbol{L}\boldsymbol{y}(t_i) \leq \mu_d \end{array} \tag{23}$$

3. Numerical evidence

The physical parameters of the system, considering the C2 string of the cello extracted from [6] are gathered in Table 1. The relation between parameters given in Table 1 and the physical parameters in Eqs. (1-3) is described in Appendix A. For all the calculation, a modal damping $\zeta = 0.1\%$ has been used for each string-body coupled modes.

The evolution of the natural frequencies of the coupled system for the parameters given in Table (1) is depicted in Fig. 2(a). Solid lines (orange) correspond to the natural frequencies of the coupled system obtained by solving Eq. (10) while dashed lines (blue) correspond to the natural frequencies of the hinged-hinged string given by Eq. (11), and adimensional frequency of the body $\omega = \sqrt{k/m}$. It is observed that frequency coalescence is avoided by the occurrence of a frequency veering phenomenon [22]. As depicted in Fig. 2(b,c), where the mode-shapes of the first two modes are plotted for $x_L = 0.33$ and $x_L = 0.4$, the veering phenomenon gives rise to modal hybridation. Close to frequency coalescence, for $x_L = 0.33$, the first two modes have comparable string amplitude and out of phase motion at the origin (i.e. bridge location) having also comparable amplitude, suggesting modal hybridation. For $x_L = 0.4$, away from frequency coalescence, the first mode shows large string displacement with small displacement at the origin, while the second mode shows comparatively small string amplitude with large bridge motion. This suggests localization of mode, the first one corresponding to string motion and the second one to body motion.

In order to perform numerical simulation of the equation of motion Eq. (12), the truncation order of the modal basis needs to be determined. It has been shown in [6] that a high number

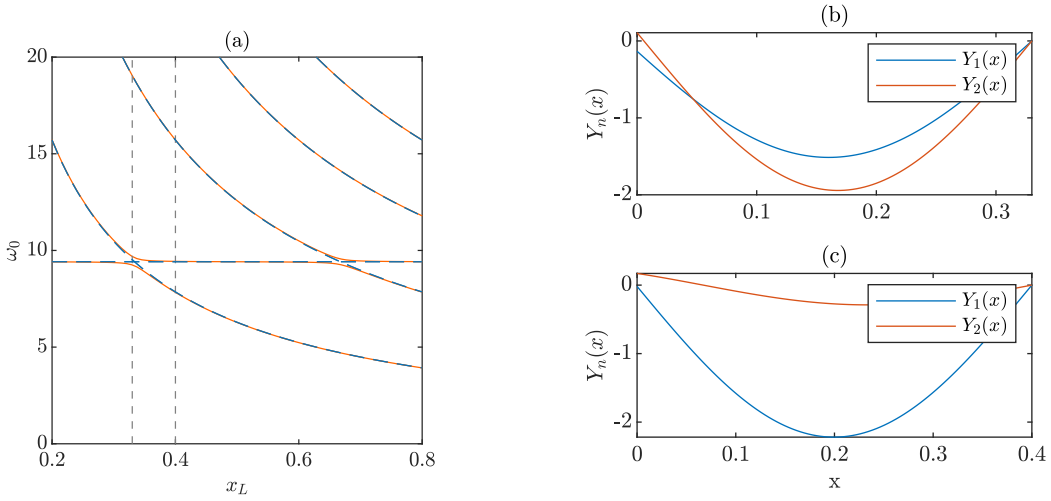

Figure 2: (a): Evolution of the natural frequencies as a function of x_L. Solid lines (orange) refer to the coupled system and dashed lines (blue) to the uncoupled system. Vertical dot-dashed lines indicate two particular values $x_L = 0.33$ and $x_L = 0.4$. (b,c): Corresponding mode shapes for $x_L = 0.33$ and $x_L = 0.4$, respectively.

of mode (80) is needed to reach computational convergence. It seems difficult if not impossible to perform numerical continuation and bifurcation analysis on such a system as suggested by the intricate bifurcation diagram of a modal model of a bowed hinged-hinged string comprising only two modes [19]. In order to investigate the effect of modal hybridation, only the first two modes have been kept in the modal discretization aiming to show the main phenomena involved in the dynamics of the system. Using the same range of playing parameters as in [6], a numerical bifurcation diagram computed for a normal bow force of $F_N = 2N$ and a bow velocity of $V_b = 0.1ms^{-1}$ is depicted in Fig. 3 for increasing and decreasing x_L around the $1:1$ string-body resonance. On the vertical axis, the points correspond to the trajectory of the bridge (i.e. $v(0,t) = \sum_n Y_n(0)v_n(t)$) intersecting the Poincaré section defined by

$$S = \{v \in \mathbb{R} : \dot{v}(0,t) = 0, v(0,t) > 0\} \tag{24}$$

Two branches of periodic solutions are observed. When x_L is increasing (blue dots in Fig. 3), the solution jumps from one stable branch to the other stable branch close to $x_L = 0.349$. The time history at the jump location is depicted in Fig. 4(a) and it is observed that the jump between the two stable periodic solutions causes deep amplitude modulation due to the low damping of the system. When x_L is decreasing (orange dots in Fig. 3), the periodic solution loses its stability giving rise to complex aperiodic motion as depicted in Fig. 4(b). In this case, the motion is weakly chaotic suggesting the presence of a strange attractor. As x_L is further decreasing, aperiodic motion is annihilated and the motion jumps back to the stable periodic branch close to $x_L = 0.334$. The above observations yield the following remarks: (i) even considering only two modes, string body interaction may give rise to stable aperiodic motion, (ii) upward or downward glissando gives rise to different behavior, (iii) even if no stable aperiodic solution is observed during the forward glissando, the jump between two stable branches yields deeply modulated motion. Note that the remarks (ii,iii) are consistent with the results of numerical simulations presented in [6] who mentions that

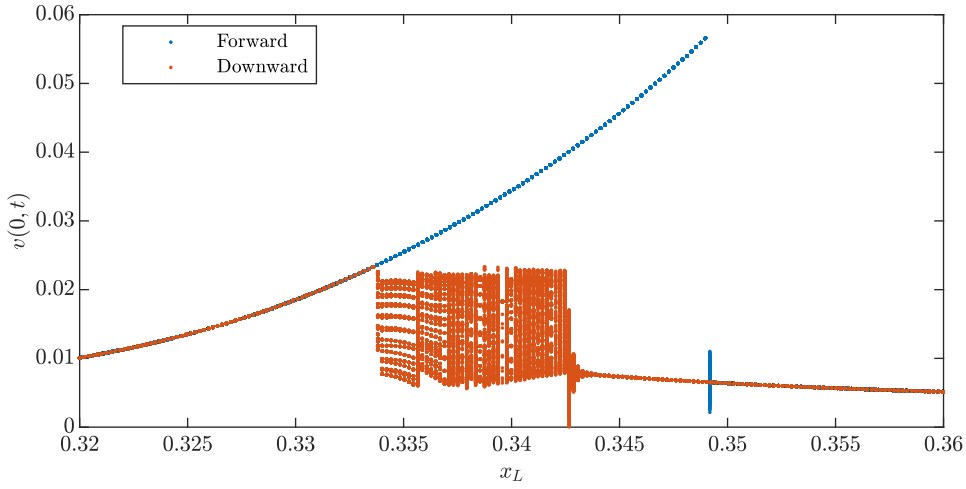

Figure 3: Numerical bifurcation diagram for parameters given in Table (1), $F_N = 2N$ and $V_b = 0.1ms^{-1}$. Forward points (blue) are obtained when x_L is increased from 0.32 to 0.36. Downward points (orange) are obtained when x_L is decreased from 0.36 to 0.32

the wolf tone does not arise at exactly the same value for the upward and downward glissando.

4. Computation of periodic solutions

The knowledge of the periodic solution and associated bifurcations gives a deep insight into the dynamics of the system. Due to the presence of Coulomb friction, the system is piecewise smooth, which prevents the use of classical methods. This problem can be addressed by using a mapping procedure [23].

4.1. Mapping

We look for periodic solutions of Eq. (12) with one slip and one stick motion per period denoted as single slip solution for brevity. It is described by

$$\begin{array}{ll} \text{slip motion from } t=0 \text{ to } t=t_1 \text{ given by (21):} & \boldsymbol{y}^I = \boldsymbol{M}(t_1)(\boldsymbol{y}_0 - \boldsymbol{p}) + \boldsymbol{p} \\ \text{stick motion from } t=t_1 \text{ to } t=t_2 \text{ given by (18):} & \boldsymbol{y}^{II} = \boldsymbol{S}(t_2)\boldsymbol{y}^I \end{array} \tag{25}$$

where $\boldsymbol{y}_0$ is the unknown initial condition vector and the unknown time instants t_1 and t_2 are be computed by taking into account slip-stick and stick-slip transition conditions such that

$$\begin{array}{ll} \text{slip stick transition given by (22):} & h_1(\boldsymbol{y}_0, t_1) \equiv \boldsymbol{h}^T\boldsymbol{y}^I - V = 0 \\ \text{stick slip transition given by (19):} & h_2(\boldsymbol{y}_0, t_1, t_2) \equiv \boldsymbol{L}\boldsymbol{y}^{II} - \mu_s = 0 \end{array} \tag{26}$$

Note that the solution is valid if $\boldsymbol{L}\boldsymbol{y}^I \leq \mu_d$ and of course

$$\begin{array}{ll} \boldsymbol{L}\boldsymbol{y}(t_1) \leq \mu_d & \\ \boldsymbol{h}^T\boldsymbol{y}(t) < V & \text{for } t \in [0, t_1[\\ |\boldsymbol{L}\boldsymbol{y}(t)| < \mu_s & \text{for } t \in [t_1, t_2[\end{array} \tag{27}$$

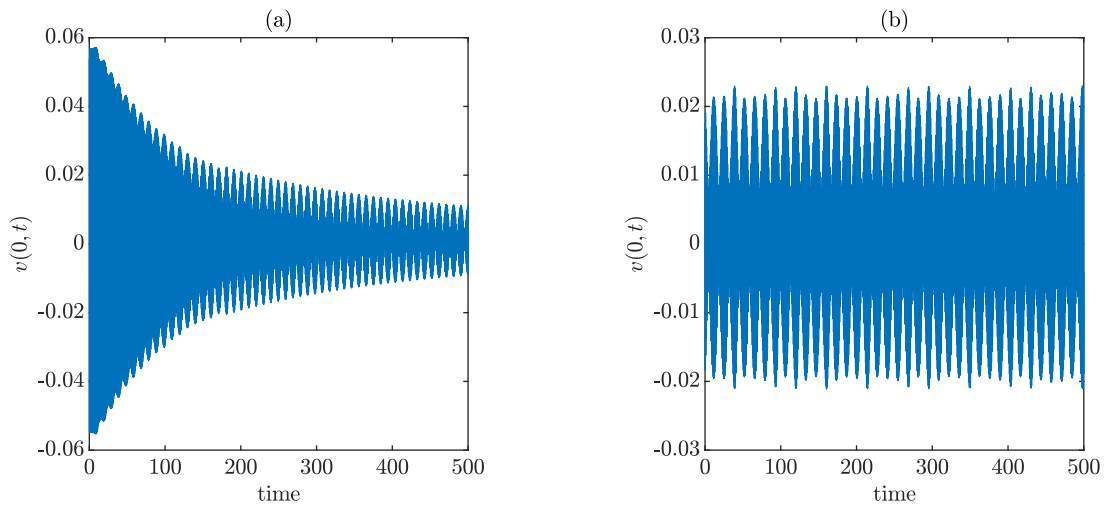

Figure 4: Time history of the bridge motion corresponding to particular points of Fig. 3. (a) $x_L = 0.349$ for increasing x_L. (b) $x_L = 0.34$ for decreasing x_L.

The first condition coming from Eq. (23) ensures that the event is a slip-stick transition and not a slip-slip transition. The second and third conditions ensure that no secondary events are present during slipping and sticking phases of the motion. Finally, periodic solutions satisfy the following condition

$$\boldsymbol{g}(\boldsymbol{y}_0, t_1, t_2) \equiv \boldsymbol{y}^{II} - \boldsymbol{y}_0 = 0 \tag{28}$$

System (26,28) is solved numerically using a Newton procedure for the triplet $(\boldsymbol{y}_0, t_1, t_2)$.

4.2. Regular bifurcation

In this section, we look for the stability of the single slip periodic solutions. This section is devoted to the analysis of classical codimension 1 bifurcations. The stability of the periodic solutions is determined by looking at the Floquet multipliers of the Poincaré return map, computed using a condensation procedure. Let us denote by $(\hat{\boldsymbol{y}}_0, \hat{t}_1, \hat{t}_2)$ a set of periodic solution. Adding perturbations yields to

$$\boldsymbol{y}_0 = \hat{\boldsymbol{y}}_0 + \delta\boldsymbol{y}_0, \quad t_1 = \hat{t}_1 + \delta t_1, \quad t_2 = \hat{t}_2 + \delta t_2 \tag{29}$$

Note that the perturbed solution must also satisfy the event conditions h_1 and h_2 in Eq. (26), such that

$$\begin{aligned} h_1(\hat{\boldsymbol{y}}_0 + \delta\boldsymbol{y}_0, \hat{t}_1 + \delta t_1) &= 0 \\ h_2(\hat{\boldsymbol{y}}_0 + \delta\boldsymbol{y}_0, \hat{t}_1 + \delta t_1, \hat{t}_2 + \delta t_2) &= 0 \end{aligned} \tag{30}$$

Substituting perturbations into Eq. (28), taking into account the previous relation and expanding the result into first order Taylor series gives

$$\begin{pmatrix} 0 \\ 0 \\ \boldsymbol{g}(\hat{\boldsymbol{y}}_0 + \delta\boldsymbol{y}_0, \hat{t}_1 + \delta t_1, \hat{t}_2 + \delta t_2) \end{pmatrix} = \boldsymbol{J} \begin{pmatrix} \delta\boldsymbol{y}_0 \\ \delta t_1 \\ \delta t_2 \end{pmatrix} \tag{31}$$

where $\boldsymbol{J}$ is the matrix of partial derivatives evaluated at the periodic solution and is given by

$$\boldsymbol{J} = \begin{bmatrix} \dfrac{\partial h_1}{\partial \boldsymbol{y}_0} & \dfrac{\partial h_1}{\partial t_1} & 0 \\ \dfrac{\partial h_2}{\partial \boldsymbol{y}_0} & \dfrac{\partial h_2}{\partial t_1} & \dfrac{\partial h_2}{\partial t_2} \\ \dfrac{\partial \boldsymbol{g}}{\partial \boldsymbol{y}_0} & \dfrac{\partial \boldsymbol{g}}{\partial t_1} & \dfrac{\partial \boldsymbol{g}}{\partial t_2} \end{bmatrix} \tag{32}$$

Removing dependencies upon δt_1 and δt_2 (condensation procedure) gives

$$\boldsymbol{g}(\hat{\boldsymbol{y}}_0 + \delta\boldsymbol{y}_0, \hat{t}_1 + \delta t_1, \hat{t}_2 + \delta t_2) = \frac{\partial \boldsymbol{g}}{\partial \boldsymbol{y}_0}\delta\boldsymbol{y}_0 - \begin{pmatrix} \dfrac{\partial \boldsymbol{g}}{\partial t_1} & \dfrac{\partial \boldsymbol{g}}{\partial t_2} \end{pmatrix} \begin{bmatrix} \dfrac{\partial h_1}{\partial t_1} & 0 \\ \dfrac{\partial h_2}{\partial t_1} & \dfrac{\partial h_2}{\partial t_2} \end{bmatrix}^{-1} \begin{pmatrix} \dfrac{\partial h_1}{\partial \boldsymbol{y}_0} \\ \dfrac{\partial h_2}{\partial \boldsymbol{y}_0} \end{pmatrix} \delta\boldsymbol{y}_0 \tag{33}$$

Substituting $\boldsymbol{g}(\hat{\boldsymbol{y}}_0 + \delta\boldsymbol{y}_0, \hat{t}_1 + \delta t_1, \hat{t}_2 + \delta t_2) = \tilde{\boldsymbol{y}}^{II} - \boldsymbol{y}_0 - \delta\boldsymbol{y}_0$, where $\tilde{\boldsymbol{y}}^{II}$ is the perturbed return point of the map, into Eq. (33) and taking the derivative with respect to the perturbation $\delta\boldsymbol{y}_0$ finally gives

$$\frac{d\tilde{\boldsymbol{y}}^{II}}{d\delta\boldsymbol{y}_0} = \boldsymbol{I} + \frac{\partial \boldsymbol{g}}{\partial \boldsymbol{y}_0} - \begin{pmatrix} \dfrac{\partial \boldsymbol{g}}{\partial t_1} & \dfrac{\partial \boldsymbol{g}}{\partial t_2} \end{pmatrix} \begin{bmatrix} \dfrac{\partial h_1}{\partial t_1} & 0 \\ \dfrac{\partial h_2}{\partial t_1} & \dfrac{\partial h_2}{\partial t_2} \end{bmatrix}^{-1} \begin{pmatrix} \dfrac{\partial h_1}{\partial \boldsymbol{y}_0} \\ \dfrac{\partial h_2}{\partial \boldsymbol{y}_0} \end{pmatrix} \tag{34}$$

Eq. (34) represents the variation of return point subjected to small perturbations, in other words, the Jacobian matrix of the Poincaré return map, whose eigenvalues are the Floquet multipliers. The periodic solution is stable when all Floquet multipliers are located inside the unit circle and unstable otherwise. When a periodic solution loses its stability, the resulting solution depends on the manner in which the Floquet multiplier leaves the unit circle [24]. A Floquet multiplier leaving the unit circle through $+1$ corresponds to a fold bifurcation, a Floquet multiplier leaving the unit circle through -1 corresponds to a flip (or period doubling) bifurcation and if a pair of complex conjugate Floquet multipliers leave the unit circle it corresponds to a Neimark-Sacker bifurcation.

4.3. Grazing bifurcation

In addition to classical bifurcations, system (6) may also encounter grazing bifurcation associated with non-smooth dynamical systems. A grazing bifurcation occurs when the flow is tangent to the transition plane. We can distinguish two types of grazing bifurcation. The first one denoted as velocity grazing bifurcation arise when slip stick transition occurs tangentially or

$$\begin{aligned} \boldsymbol{h}^T\boldsymbol{y} &= V \\ \boldsymbol{h}^T\dot{\boldsymbol{y}} &= 0 \end{aligned} \tag{35}$$

The second type of grazing bifurcation, denoted as force grazing bifurcation and occurs when stick slip transition is tangent as

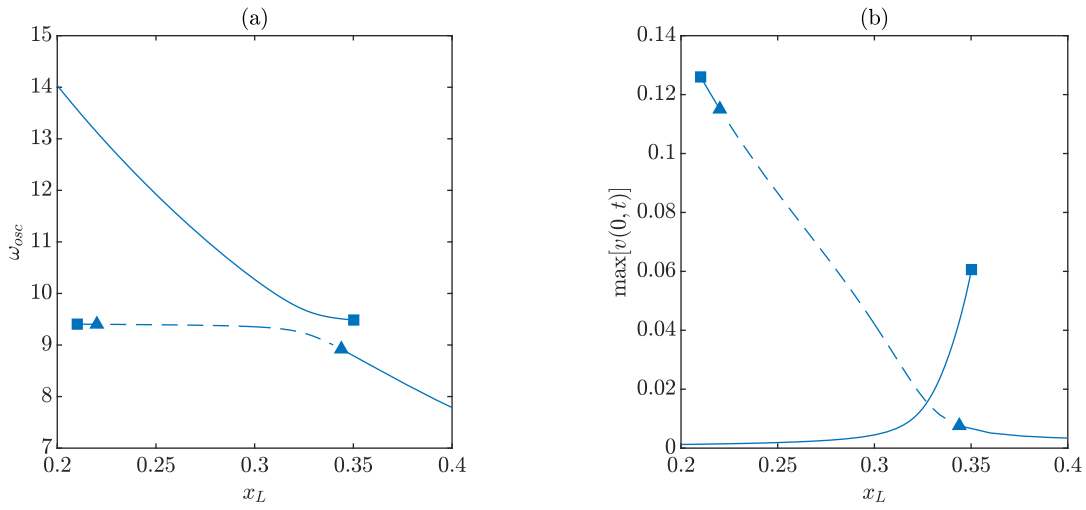

Figure 5: Bifurcation diagram of periodic stick-slip regimes for parameters given in Table (1), $F_N = 2N$ and $V_b = 0.1ms^{-1}$. Triangles and squares correspond to Neimark-Sacker and Grazing bifurcations, respectively. Solid and dashed lines correspond to stable and unstable solutions, respectively.

$$\begin{aligned} \boldsymbol{Ly} &= \pm\mu_S \\ \boldsymbol{L\dot{y}} &= 0 \end{aligned} \tag{36}$$

The computation of periodic stick slip regimes as well as the stability analysis have been embedded in a pseudo-arclength continuation scheme [25] to track branches of periodic solutions. The continuation of bifucation points has also been implemented using the minimally extended system approach described in [25].

5. Bifurcation behavior near the wolf note

The periodic solutions and associated bifurcations near 1 : 1 string body resonance are now analyzed. The bifurcation diagram of periodic stick slip regimes obtained using the same bowing parameters as those used for the numerical bifurcation diagram in Fig. 3 is depicted in Fig. 5. Solid and dashed lines correspond to stable and unstable periodic solution, respectively, and triangles and squares indicate Neimark-Sacker and velocity grazing bifurcation, respectively. Figures 5(a) and (b) are two different representations of the same result. Figure 5(a) shows the evolution of the pulsation of the stick-slip oscillation ($\omega_{osc} = 2\pi/(t_1 + t_2)$) while Fig. 5(b) shows the evolution of the maximum amplitude of the motion at the bridge. Comparison between Fig. 5(a) and Fig. 2(a) shows that the frequency of the stick slip oscillations follows the natural frequency of the system. Figure 5(b) can be directly compared to Fig. 3. As a first general remark, the periodic solutions are divided in two distinct branches. A first branch is entirely stable and stops at $x_L = 0.35$ due to a grazing bifurcation. The second presents a pair of Neimark-Sacker bifurcations at $x_L = (0.22, 0.344)$ between which the periodic solutions are unstable. The branch vanishes at $x_L = 0.21$ due to the presence of a grazing bifurcation. The presence of these bifurcations explains the behavior observed with numerical simulations in Fig. 3.

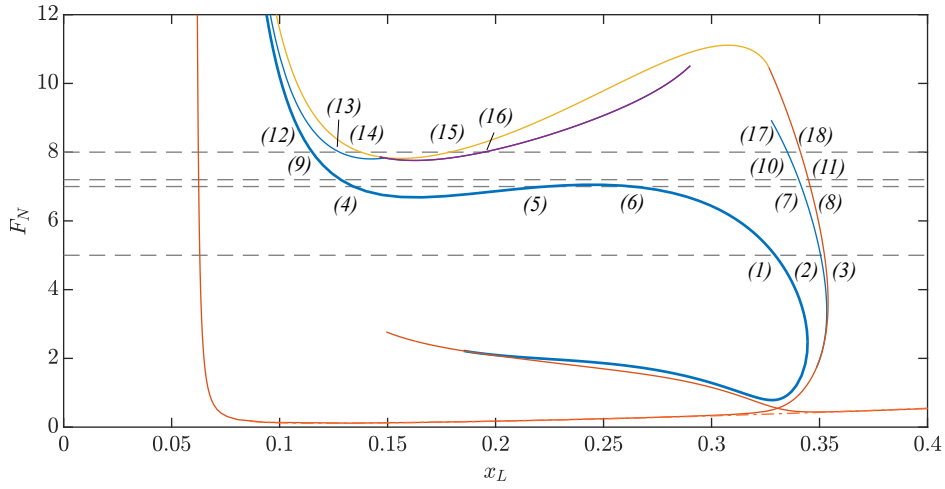

Figure 6: Locus of the bifurcation points in the (x_L, F_N) plane for parameters given in Table (1) and $V_b = 0.1ms^{-1}$. Orange lines correspond to velocity grazing bifurcation, blue lines to Neimark-Sacker bifurcation, purple lines to flip bifurcation and yellow lines to force grazing bifurcation.

A wider picture of the system dynamics is depicted in Fig. 6 where the locus of the bifurcation points is depicted in the (x_L, F_N) plane for the parameters given in Table (1) and $V_b = 0.1ms^{-1}$. Orange lines correspond to velocity grazing bifurcation, blue lines (bold and thin) to Neimark-Sacker bifurcation, purple lines to flip bifurcation and yellow lines to force grazing bifurcation. This bifurcation diagram is more easily understood by making the parallel with classical bifurcation diagram depicted in Fig. 7 where the same system parameters are used and only the bow normal force F_N is changed, as indicated by the horizontal dashed lines in Fig. 6. The italic numbers indicate the bifurcation points to facilitate the comparison between Fig. 6 and Fig. 7.

The same notation as in Fig. 5 has been used and cross and circles corresponds to flip and force grazing bifurcations, respectively. When comparing Fig. 5(b) and Fig. 7(a) (F_N has increased from $2N$ to $5N$), we observe that the small portion of stable branch for $x_L \in [0.21, 0.22]$ does not exist any more, and a Neimark-Sacker bifurcation point (labeled *(2)*) has emerged on the right stable branch corresponding to large amplitude motion of the bridge. Increasing the bow force to $F_N = 7N$ (Fig. 7(b)), a new pair of Neimark-Sacker bifurcations appears on the lower branch (labeled *(4)* and *(5)*) yielding to a stable portion of periodic stick-slip regime. Increasing the bow force to $F_N = 7.2N$, a pair of Neimark-Sacker bifurcation is destroyed. The lower branch is now almost entirely stable and two stable periodic solutions coexist over a large range of x_L. Again, increasing the normal bow force to $F_N = 8N$, the upper branch splits into two branches due to the appearance of a force grazing bifurcation (labeled *(14)* and *(15)*). It is also observed that large bow force also gives rise to flip bifurcations (labeled *(16)*).

From the above results, it is tempting to make a parallel between the minimum bow force that limits the existence of stick-slip periodic oscillations, generally used to explain the occurrence of the wolf tone, and the bifurcations of periodic solutions. Note that if the dynamic of the body is ignored by considering one string mode with hinged-hinged boundary conditions, the only bifurcation that limits the existence of single slip motion is the grazing bifurcation depicted by the

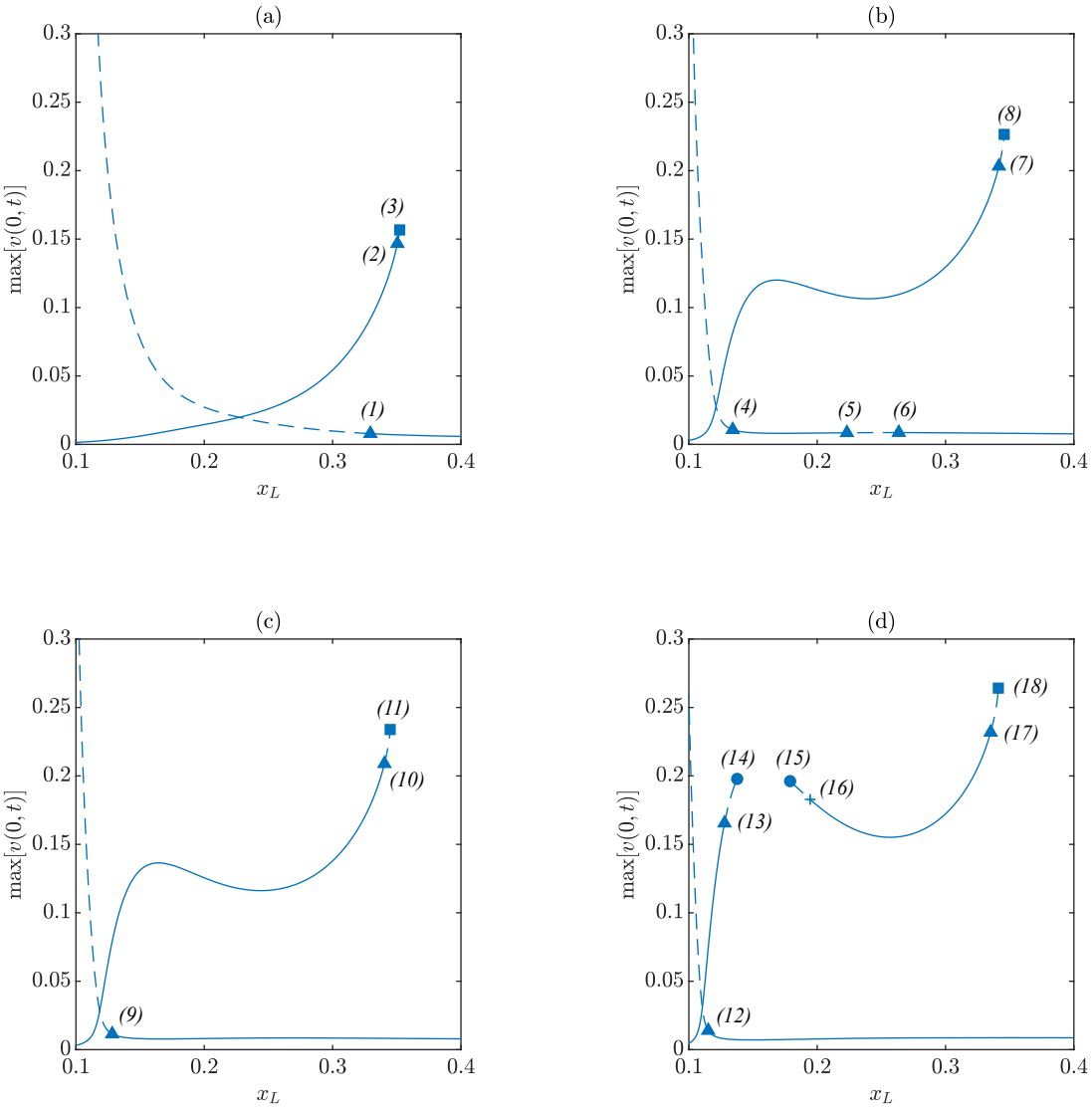

Figure 7: Bifurcation diagram of periodic stick slip regimes for parameters given in Table (1), $V_b = 0.1ms^{-1}$. (a): $F_N = 5$, (b): $F_N = 7$, (c): $F_N = 7.2$ and (d): $F_N = 8$. Triangles and squares correspond to Neimark-Sacker and velocity grazing bifurcations, respectively, cross and circles to flip and force grazing bifurcations, respectively. Solid and dashed lines corresponds to stable and unstable solutions, respectively.

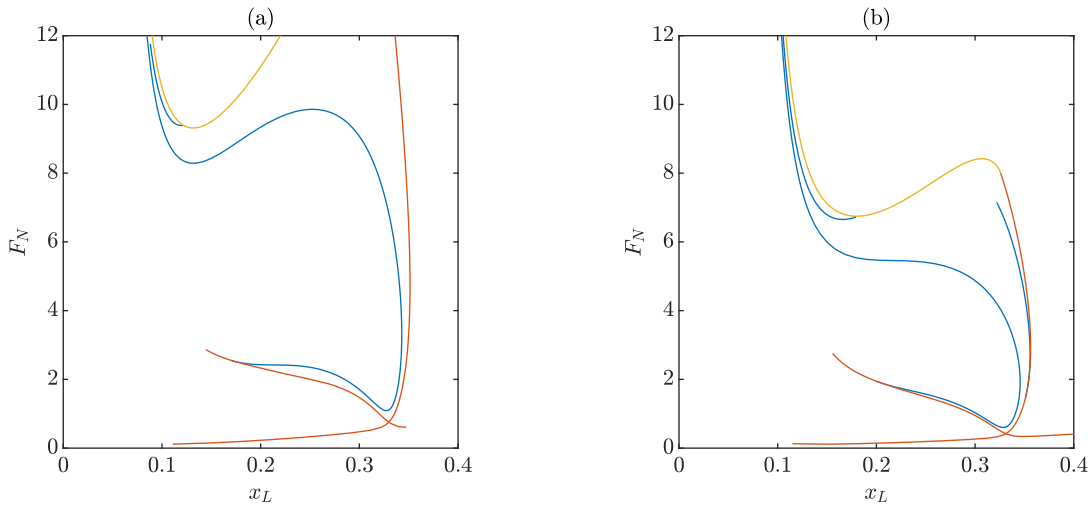

Figure 8: Locus of the bifurcation points in the (x_L, F_N) plane for parameters given in Table (1) and $V_b = 0.1ms^{-1}$. (a): $x_B = 0.5$ and (b): $x_B = 0.7$. Orange lines correspond to velocity grazing bifurcation, blue lines to Neimark-Sacker bifurcation and yellow lines to force grazing bifurcation.

orange dash-dotted line in Fig. 6. It is observed that the locus of velocity grazing bifurcation in the coupled and uncoupled case is similar except close to the frequency coalescence between the string and the body resonance. The situation changes if we consider the dynamics of the coupled system. Let us consider that the player is performing a downward glissando, decreasing x_L from 0.4. According to Fig. 7, single slip motion will lose its stability subsequent to the Neimark-Sacker bifurcation indicated by the bold blue line in Fig. 6. However, due to the S-shaped look of the Neimark-Sacker bifurcation curve, a small increase of the bow force from $F_N = 7$ (Fig. 7(b)) to $F_N = 7.2$ (Fig. 7(c)) greatly extends the stability range of single slip motion. The bow force at which this sudden increase of the playability domain occurs can be viewed as the minimum bow force under which the wolf tone phenomenon takes place.

The classical Schelleng's minimum bow force diagram, shows that the minimum bow force increases when the bridge-bow distance (denoted by x_B in the present model) decreases [3]. Figure 8, depicting the locus of the bifurcation points (similar as in Fig. 6) for different values of x_B, shows a similar trends. Although the diagrams presented in Fig. 6 and in Fig. 8 clearly present similarities, interesting changes are noticed. The stable portion of branch observed in Fig. 7(b), which is due to the horizontal S-shaped Neimark-Sacker bifurcation curve, exists for a larger range of normal bow force when x_B diminishes but vanishes when $x_B = 0.7$, showing a more complex dependence upon the bow bridge distance than suggested by Schelleng's diagram, as already mentioned by Mansour [10].

6. Conclusion

The bifurcation behavior of a simple model of cello played in the wolf region has been investigated. The model consists of a two mode modal decomposition of a linear string, subjected to a coulomb friction force, terminated at its end with a mass spring oscillator representing the dynamic of the body. It is shown that exact frequency coalescence between the frequency of the

string and the body is avoided by a veering phenomenon. The mode shape at the veering region shows hybrid mode with comparable string amplitude and out of phase motion of the body. Numerical simulations show the existence of jumps phenomenon close to $1:1$ string body resonance as well as the existence of stable quasi-periodic responses. A mapping procedure that allows to compute the periodic solution and the stability of single slip motion hes been presented. This mapping procedure has been embedded in a continuation procedure allowing us to track branch of periodic solutions as well as branch of bifurcation points. Two scenario giving rise to warbling oscillation are explained by bifurcation of periodic solution. (i) a periodic solution will lose its stability subsequent to a grazing bifurcation and jump to the competing stable branch, causing transient modulation. (ii) the periodic solution loses its stability due to the presence of a Neimark-Sacker bifurcation that can give rise to stable quasi-periodic response. Finally, it is shown that the presence of these bifurcation limits the range of possible single slip motion giving a novel interpretation of minimum bow force criterion. Although the model used in this paper is greatly simplified, the use of dedicated nonlinear tools to analyze the motion of bowed string instruments can provide interesting information about the behavior of these systems.

Acknowledgements

This work has been carried out in the framework of the Labex MEC (Contract No. ANR-10-LABX-0092) and of the A*MIDEX project (Contract No. ANR-11-IDEX- 0001-02), funded by the Investissements d'Avenir French Government program managed by the French National Research Agency (ANR).

Appendix A. Expression of physical parameters from parameter given in Table 1

The physical parameters of system Eqs. (1-3) are not directly obtained from the identified parameters of the C2 string of a cello given in Table 1 and extracted from [6]. The pre-stress tensile force N is related to the natural pulsation ω_{string} and full length L of the string as follows

$$\omega_{string} = \frac{\pi}{L}\sqrt{\frac{N}{\rho}} \tag{A.1}$$

In order to obtain meaningful values for the mass m and stiffness k of the body, used in the expression of the mechanical boundary conditions (3), the main body resonance mobility peak has been fitted by a damped spring-mass oscillator. The natural pulsation ω_{body}, damping ratio ζ_{body} and amplitude of the mobility peak M_{body} are related to the mass m, stiffness k and damping c of the equivalent damped harmonic oscillator as follows

$$\omega_{body} = \sqrt{\frac{k}{m}}, \quad \zeta_{body} = \frac{c}{2\sqrt{km}}, \quad M_{body} = \frac{1}{c} \tag{A.2}$$

Solving Eq. (A.2) for m and k gives

$$m = \frac{1}{2M_{body}\zeta_{body}\omega_{body}}, \quad k = \frac{\omega_{body}}{2M_{body}\zeta_{body}} \tag{A.3}$$

The non-dimensional parameters used for computations are then obtained by using Eq. (4).

References

[1] G. White, The origin of the wolf-note in bowed string instruments, in: Proc. Cambridge Phil. Soc, Vol. 18, 1915, p. 85.

[2] C. Raman, Xliii. on the "wolf-note" in bowed stringed instruments, The London, Edinburgh, and Dublin Philosophical Magazine and Journal of Science 32 (190) (1916) 391–395.

[3] J. Schelleng, The bowed string and the player, The Journal of the Acoustical Society of America 53 (1) (1973) 26–41.

[4] J. Woodhouse, On the playability of violins. part ii: Minimum bow force and transients, Acta Acustica united with Acustica 78 (3) (1993) 137–153.

[5] J. Woodhouse, P. Galluzzo, The bowed string as we know it today, ACTA Acustica united with Acustica 90 (4) (2004) 579–589.

[6] O. Inácio, J. Antunes, M. Wright, Computational modelling of string–body interaction for the violin family and simulation of wolf notes, Journal of Sound and Vibration 310 (1-2) (2008) 260–286.

[7] V. Debut, J. Antunes, O. Inacio, What can we learn about the wolf phenomenon from a linearized analysis?, in: Acoustics 2012, 2012.

[8] V. Debut, O. Inácio, T. Dumas, J. Antunes, Modelling and experiments on string/body coupling and the effectiveness of a cello wolf-killing device, ISMA2010 proceedings, Katoomba (2010).

[9] H. Mansour, J. Woodhouse, G. Scavone, Enhanced wave-based modelling of musical strings. part 2: Bowed strings, Acta Acustica united with Acustica 102 (6) (2016) 1094–1107.

[10] H. Mansour, J. Woodhouse, G. Scavone, On minimum bow force for bowed strings, Acta Acustica united with Acustica 103 (2) (2017) 317–330.

[11] F. Friedlander, On the oscillations of a bowed string, in: Mathematical Proceedings of the Cambridge Philosophical Society, Vol. 49, Cambridge University Press, 1953, pp. 516–530.

[12] J. Woodhouse, On the stability of bowed string motion, Acta Acustica united with Acustica 80 (1) (1994) 58–72.

[13] J. Sieber, K. Engelborghs, T. Luzyanina, G. Samaey, D. Roose, Dde-biftool manual-bifurcation analysis of delay differential equations, arXiv preprint arXiv:1406.7144 (2014).

[14] S. Terrien, C. Vergez, B. Fabre, Flute-like musical instruments: a toy model investigated through numerical continuation, Journal of sound and vibration 332 (15) (2013) 3833–3848.

[15] S. Karkar, C. Vergez, B. Cochelin, Oscillation threshold of a clarinet model: A numerical continuation approach, The Journal of the Acoustical Society of America 131 (1) (2012) 698–707.

[16] T. Colinot, P. Guillemain, C. Vergez, J.-B. Doc, P. Sanchez, Multiple two-step oscillation regimes produced by the alto saxophone, The Journal of the Acoustical Society of America (2020).

[17] J. Gilbert, S. Maugeais, C. Vergez, Minimal blowing pressure allowing periodic oscillations in a simplified reed musical instrument model: Bouasse-benade prescription assessed through numerical continuation, Acta Acustica (2020).

[18] V. Fréour, L. Guillot, H. Masuda, S. Usa, E. Tominaga, Y. Tohgi, C. Vergez, B. Cochelin, Numerical continuation of a physical model of brass instruments: Application to trumpet comparisons, The Journal of the Acoustical Society of America (2020).

[19] P. Vigué, B. Cochelin, C. Vergez, K. Sami, Investigation of periodic solutions of a bowed string toy model, in: Congrès français de mécanique, AFM, Association Française de Mécanique, 2015.

[20] L. Guillot, B. Cochelin, C. Vergez, A generic and efficient taylor series–based continuation method using a quadratic recast of smooth nonlinear systems, International Journal for Numerical Methods in Engineering 119 (4) (2019) 261–280.

[21] Y. Kuznetsov, S. Rinaldi, A. Gragnani, One-parameter bifurcations in planar filippov systems, International Journal of Bifurcation and chaos (2003).

[22] N. Perkins, C. Mote, Comments on curve veering in eigenvalue problems, Journal of Sound and Vibration 106 (3) (1986) 451–463.

[23] S. Lenci, G. Rega, Periodic solutions and bifurcations in an impact inverted pendulum under impulsive excitation, Chaos, Solitons & Fractals 11 (15) (2000) 2453–2472.

[24] A. Nayfeh, B. Balachandran, Applied nonlinear dynamics: analytical, computational, and experimental methods, John Wiley & Sons, 2008.

[25] Y. Kuznetsov, Elements of applied bifurcation theory, Vol. 112, Springer Science & Business Media, 2013.